A Numerical Approach to Modeling the Catalytic Voltammetry of Surface-Confined Redox Enzymes

Michael J. Honeychurch* and Paul V. Bernhardt*

Centre for Metals in Biology, Department of Chemistry, University of Queensland, Brisbane 4072, Australia

Received: May 21, 2004; In Final Form: July 13, 2004

A finite difference method for simulating voltammograms of electrochemically driven enzyme catalysis is presented. The method enables any enzyme mechanism to be simulated. The finite difference equations can be represented as a matrix equation containing a nonlinear sparse matrix. This equation has been solved using the software package Mathematica. Our focus is on the use of cyclic voltammetry since this is the most commonly employed electrochemical method used to elucidate mechanisms. The use of cyclic voltammetry to obtain data from systems obeying Michaelis−Menten kinetics is discussed, and we then verify our observations on the Michaelis−Menten system using the finite difference simulation. Finally, we demonstrate how the method can be used to obtain mechanistic information on a real redox enzyme system, the complex bacterial molybdoenzyme xanthine dehydrogenase.

Introduction

The use of electrochemical methods to study the electron-transfer reactions of proteins and enzymes is well developed.[1] Objectives of electrochemical protein research vary, but a large proportion of published work is oriented either directly or indirectly to amperometric biosensor applications. Such devices measure an electrochemical current generated through the enzymatic (catalytic) oxidation or reduction of an analyte, which is correlated with analyte concentration. The benchmark in this field is the glucose oxidase electrode,[2] first developed by Hill and co-workers, which has claims to being the most commonly used analytical device in the world. It is now used routinely throughout the world by diabetics for rapid and accurate measurement of blood glucose concentrations.[3] Similar devices for the accurate analysis of other biologically important molecules will continue to emerge in the years to come as more redox enzymes are characterized.

The relation between the catalytic current and substrate concentration often obeys Michaelis−Menten kinetics, i.e., the current varies nonlinearly with substrate concentration and approaches a saturating (enzyme-limited) value at concentrations well in excess of the Michaelis constant (K_m). Therefore, bio-analytical applications are reliant upon the catalytic electrochemistry of the protein being well understood, which includes determination of its fundamental steady-state kinetic parameters such as K_m and the turnover number, which equates in electrochemical terms to the saturating catalytic current.

Heterogeneous electron transfer, between an electrochemical working electrode and a protein redox center, often remote from the surface, is nontrivial, and the problem is further complicated when catalytic chemical reactions are coupled to electron transfer in redox enzymes. Indeed the number of redox enzymes that have been successfully studied by direct electrochemistry (without the use of artificial electron transfer relays or mediators) is still relatively small, and for this reason, theoretical studies of the response of electrochemically driven enzyme catalysis have generally focused on mediated systems.[4−9] In cases where theoretical studies of unmediated systems are reported, the objective is usually to obtain closed-form analytical solution(s) to explain the problem being studied. This generally requires some restrictive simplifying assumptions, even for relatively uncomplicated mechanisms. One of the typical assumptions in catalytic enzyme electrochemistry is that of a steady state, i.e., the concentration of the enzyme−substrate complex remains constant throughout catalysis which demands that the concentration of free substrate near the electrode surface is also unchanged. However, if a steady-state substrate concentration is not achieved, as is often the case in transient electrochemical techniques such as cyclic voltammetry where the concentration of substrate may be depleted near the electrode surface, the closed form solution obtained is a Volterra equation of the second kind, which must be solved numerically.

In this context, our approach here is to seek a numerical solution to the governing equations directly rather than pursuing an ultimately (numerically obtained) closed form analytical solution that relies on assumptions, which may break down under certain conditions. We will set out the differential equations describing the system and solve these equations by a fully implicit finite difference (FIFD) method.[10−13] We present a general numerical method for simulating electrochemically driven enzyme-catalyzed reactions in which the enzyme is confined to the electrode surface and both the substrate and its product are soluble. No mechanistic simplifications are required, and in fact, the numerical method enables the analytical solutions to be tested so as to determine under what conditions the simplifying assumptions made in their derivations break down.

Redox enzyme catalysis by nature involves a series of sequential electrochemical and chemical reactions, each governed by its own intrinsic kinetic and thermodynamic constants. As the number of mechanistic steps increases, the number of parameters rises accordingly and an unambiguous determination through simulation may not be possible, regardless of whether

* To whom correspondence may be addressed. E-mail: m.honeychurch@uq.edu.au (M.J.H.); p.bernhardt@uq.edu.au (P.V.B.).

10.1021/jp047808g CCC: $27.50
Published on Web 09/14/2004

numerical or analytical methods are employed to attempt to simulate the system. Such situations call for estimates of parameter values from, e.g., the biochemical literature if they are available.

Below we introduce the theory underpinning the fully implicit finite difference approach to simulations of electrochemically driven enzyme catalytic systems. Our focus in this paper is on the use of cyclic voltammetry since this is the most commonly employed electrochemical method used to elucidate mechanisms. We then briefly discuss the use of cyclic voltammetry to obtain data from systems obeying Michaelis−Menten kinetics. We verify our observations on the Michaelis−Menten system using the finite difference simulation. Finally we demonstrate how the method can be used to obtain mechanistic information on a complex redox enzyme system, the bacterial molybdoenzyme xanthine dehydrogenase (XDH).

Theory

Consider an enzyme catalytic reaction consisting of n reaction steps where the subscript indicates the species number of the various forms of the surface-bound enzyme, E, and S and P are the substrate and product, respectively. The rate constant k_{ij} refers to the first-order or pseudo-first-order reaction in which form i of the enzyme goes to form j. Transformation of particular steps to second order is described further below. The total electroactive enzyme surface concentration, Γ_T, is assumed to be constant during the experiment therefore

$$\sum_i \Gamma_i = \Gamma_T \tag{1}$$

with Γ_i as the surface concentration of form i of the enzyme. Dividing through by Γ_T gives

$$\sum_i x_i = 1 \tag{2}$$

and differentiating eq 2 gives

$$\sum_i \frac{dx_i}{dt} = 0 \tag{3}$$

The rate equation can be written in matrix form, $d\boldsymbol{x}/dt = \boldsymbol{A}\boldsymbol{x}$, as

$$\frac{d}{dt}\begin{bmatrix} x_1 \\ x_2 \\ \vdots \\ x_i \\ \vdots \\ x_{n-1} \\ x_n \end{bmatrix} = \begin{bmatrix} -(k_{1n}+k_{12}) & k_{21} & & 0 & & & & 0 & & k_{n1} \\ k_{12} & -(k_{21}+k_{23}) & \ddots & k_{32} & 0 & & & & & 0 \\ 0 & \ddots & \ddots & \ddots & \ddots & & & & & \vdots \\ \vdots & & & & k_{(i-1)i} & -(k_{i(i-1)}+k_{i(i+1)}) & k_{(i+1)i} & & & \vdots \\ \vdots & & & & & \ddots & \ddots & \ddots & & 0 \\ 0 & & & & 0 & & k_{(n-2)(n-1)} & -(k_{(n-1)(n-2)}+k_{(n-1)n}) & k_{n(n-1)} & \\ k_{1n} & 0 & & \cdots & & & 0 & k_{(n-1)n} & -(k_{n(n-1)}+k_{n1}) & \end{bmatrix} \begin{bmatrix} x_1 \\ x_2 \\ \vdots \\ x_i \\ \vdots \\ x_{n-1} \\ x_n \end{bmatrix} \tag{4}$$

SCHEME 1

$$E_1 \underset{k_{21}}{\overset{k_{12}}{\rightleftharpoons}} E_2$$

$$E_2 \underset{k_{32}}{\overset{k_{23}}{\rightleftharpoons}} E_3$$

$$\vdots$$

$$E_i + S \underset{k_{(i+1)i}}{\overset{k_{i(i+1)}}{\rightleftharpoons}} E.S_{i+1}$$

$$\vdots$$

$$E.S_{n-1} \underset{k_{n(n-1)}}{\overset{k_{(n-1)}}{\rightleftharpoons}} E.P_n$$

$$E.P_n \underset{k_{1n}}{\overset{k_{n1}}{\rightleftharpoons}} E_1 + P$$

where $\boldsymbol{x}$ is the vector of fractional concentrations of the various forms of the enzyme and $\boldsymbol{A}$ is the matrix of rate constants. For voltammetrically driven enzyme catalysis, several of the rate constants present in $\boldsymbol{A}$ will be time/potential dependent and the concentration of substrate at the electrode surface, $c_S(x,t)$, will differ from the bulk concentration of substrate, c_S^*, as shown for example in Figure 1.

In Scheme 1, the rate constant, $k_{i(i+1)}$ is the product of a second-order rate constant $k'_{i(i+1)}$ and the concentration (strictly speaking, the activity) of the substrate at the electrode surface. Likewise the rate constant k_{1n} will comprise the product of a second-order rate constant, k'_{1n},, and the concentration of the product at the electrode surface. The concentration of substrate at the electrode surface can be determined from solving the equations of Fick's first and second laws

$$-J_S(x,t) = D_S\left(\frac{\partial c_S(x,t)}{\partial x}\right) \tag{5}$$

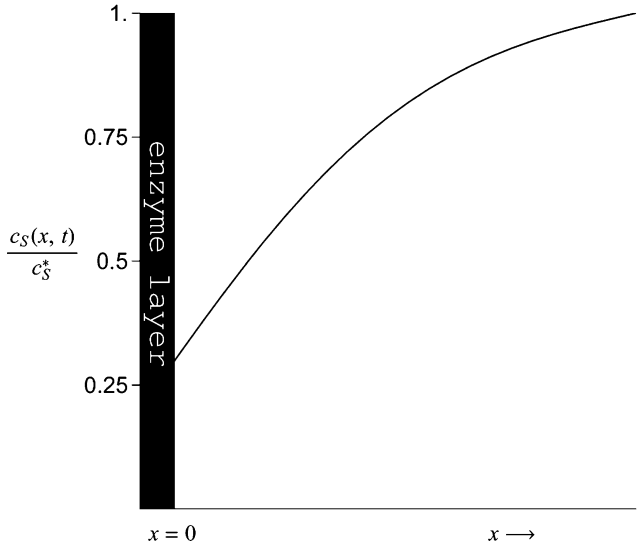

Figure 1. Example of the concentration gradient that arises during an electrochemical experiment.

$$\frac{\partial c_S(x,t)}{\partial t} = D_S \frac{\partial^2 c_S(x,t)}{\partial x^2} \tag{6}$$

where $J_S(x,t)$ is the flux of substrate at a distance x from the electrode surface, $c_S(x,t)$ the concentration of the substrate, and D_S the diffusion coefficient of the substrate, with the initial condition and boundary conditions being

$$c_S(x,0) = c_S^* \tag{7}$$

$$c_S(\infty,t) = c_S^* \tag{8}$$

$$-J_S(0,t) = D_S\left(\frac{\partial c_S(x,t)}{\partial x}\right)_{x=0} = k'_{i(i+1)}c_S(0,t)\Gamma_i - k_{(i+1)i}\Gamma_{i+1} \tag{9}$$

In some circumstances, such as a very sparse coverage of enzyme, diffusion to an isolated enzymes sites would be approximately spherical.[14] To model such cases, the spherical version of eq 6 would have to be used. If spherical diffusion to isolated sites were to be assumed, the spherical version of eq 6 could be converted into a linear form by making the transformation $u(r,t) = rc_S(r,t)$ (see ref. 15 for more details on this approach). This would render the mathematical approach needed to solve such a system as being analogous to that described for the linear case below.

The solution is[15]

$$c_S(0,t) = c_S^* - \frac{1}{(\pi D_S)^{1/2}}\int_0^t J_S(0,u)(t-u)^{-1/2}\,du \tag{10}$$

This equation must be solved numerically. Likewise, the flux of product at the electrode surface is

$$-J_P(0,t) = D_P\left(\frac{\partial c_P(x,t)}{\partial x}\right)_{x=0} = k'_{1n}c_P(0,t)\Gamma_1 - k_{n1}\Gamma_n \tag{11}$$

The current generated will be equal to the current from the redox reactions of cofactors within the enzyme plus the catalytic current, i_{cat}, from substrate turnover

$$i(t) = FA\sum_j n_j \frac{d\Gamma_j}{dt} + i_{cat}(t) \tag{12}$$

In eq 12, n_j is the number of electrons transferred in the jth reaction step of Scheme 1. The catalytic current density, j_{cat}, due to the substrate turnover (product formation), is

$$j_{cat}(t) = D_P\left(\frac{\partial c_P(x,t)}{\partial x}\right)_{x=0} = n_P F c_S^*(\pi D_P \sigma)^{1/2}\chi \tag{13}$$

where σ is the dimensionless sweep rate ($n_P F\upsilon/RT$), with υ being the sweep rate, and χ is the dimensionless current function[15]

$$\chi(\sigma t) = \frac{1}{\pi}\int_0^{\sigma t}\frac{1}{(\sigma t - z)^{1/2}}\left(\frac{dg(\sigma t)}{d(\sigma t)}\right)_\sigma t = z\,dz \tag{14}$$

where $g(\sigma t) = 1 - (c_P(0,t)/c_S^*)$.

The current density, j, due to the electrochemical reaction of an adsorbed molecule is[16,17]

$$j(t) = -n_j F\upsilon\Gamma_T\left(\frac{F}{RT}\right)\psi_j \tag{15}$$

where ψ is the dimensionless current for adsorbed molecules defined as

$$\psi_j = -\frac{RT}{F}\frac{dx_j}{dE} \tag{16}$$

The total current density for the reaction is the sum of the current densities from the electrochemical reactions of redox cofactors within the enzyme and the catalytic current

$$j(t) = \upsilon\Gamma_T\frac{F^2}{RT}\sum_j n_j\psi_j - n_P F c_S^*(\pi D_P\sigma)^{1/2}\chi \tag{17}$$

(i) Michaelis−Menten Kinetics. For the homogeneous solution reaction

$$E + S \underset{k_{-1}}{\overset{k_{+1}}{\rightleftharpoons}} ES \xrightarrow{k_2} E + P \tag{18}$$

the Michaelis constant, derived under the steady-state assumption that $d[ES]/dt \cong 0$, is defined as

$$K_m = \frac{(k_{-1} + k_2)}{k_{+1}} \tag{19}$$

In the biochemical literature the rate, υ, of product formation is given as

$$\upsilon = \frac{d[P]}{dt} = \frac{k_2[E_T][S]}{K_m + [S]} \tag{20}$$

where $[E_T] = [E] + [ES]$.

In electrochemically driven enzyme catalysis, where the active enzyme exists as a monolayer or submonolayer on the electrode surface, in its simplest form, eq 18 can be rewritten as

$$E' \xrightarrow{k_s} E + S \underset{k_{-1}}{\overset{k_{+1}}{\rightleftharpoons}} ES \xrightarrow{k_2} E + P \tag{21}$$

In this scheme, the enzyme E′ is converted into an active form electrochemically with a standard electrochemical rate constant k_s. The flux of product at the electrode surface for eq 21 is

$$-J_P(0,t) = D_P\left(\frac{\partial c_P(x,t)}{\partial x}\right)_{x=0} = -k_2\Gamma_{ES} \quad (22)$$

Since the greatest concentration of P will be at the electrode surface, the concentration gradient is negative. Typically an expression for Γ_{ES} is derived from the rate equations by applying the steady-state assumption, which yields

$$\Gamma_{ES} = \frac{(\Gamma_T - \Gamma_{E'})c_S(0,t)}{K_m + c_S(0,t)} \quad (23)$$

Therefore

$$D_P\left(\frac{\partial c_P(x,t)}{\partial x}\right)_{x=0} = -k_2\frac{(\Gamma_T - \Gamma_{E'})c_S(0,t)}{K_m + c_S(0,t)} = \frac{i_{cat}(t)}{nFA} \quad (24)$$

where i_{cat} is the catalytic current. Hence the electrochemical version of the Michaelis−Menten rate expression is

$$i_{cat}(t) = \frac{nFAk_2(\Gamma_T - \Gamma_{E'})c_S(0,t)}{K_m + c_S(0,t)} \quad (25)$$

In practice, "apparent" K_m and k_2 values are obtained by plotting the background-subtracted current vs c_S^* and Γ_T is used rather that $(\Gamma_T - \Gamma_{E'})$, which is not known.

Given that the amount of S existing as ES is assumed to be constant (and negligible), the flux of S should be equal in magnitude and opposite in sign to the flux of P. It is evident from eq 23 that the steady-state assumption will only be valid if the catalytic current is constant, and any departure from a constant current indicates that this assumption is invalid. Equation 25 allows the K_m value to be determined from a plot of catalytic current vs surface concentration of the substrate, which is given in eq 10 and can be rewritten in terms of the catalytic current as

$$c_S(0,t) = c_S^* - \frac{1}{nFA(\pi D_S)^{1/2}}\int_0^t i_{cat}(u)(t-u)^{-1/2}\,du \quad (26)$$

Thus, eq 26 allows the surface concentration, as opposed to the bulk concentration, of substrate to be determined, and when substituted into eq 25, the actual (as opposed to apparent) K_m and k_2 values emerge. The Riemann−Liouville definition of a semi-integral (where the differentiation of negative order is equivalent to integration) is[18]

$$\frac{d^{(-1/2)}}{dt^{(-1/2)}}f(t) = \frac{1}{\pi^{1/2}}\int_0^t f(u)(t-u)^{-1/2}\,du \quad (27)$$

Therefore eq 26 becomes

$$c_S(0,t) = \frac{1}{nFAD_S^{1/2}}\frac{d^{(-1/2)}}{dt^{(-1/2)}}i_{cat}(t) \quad (28)$$

Likewise the concentration of product at the electrode surface is

$$c_P(0,t) = \frac{1}{nFAD_P^{1/2}}\frac{d^{(-1/2)}}{dt^{(-1/2)}}i_{cat}(t) \quad (29)$$

SCHEME 2

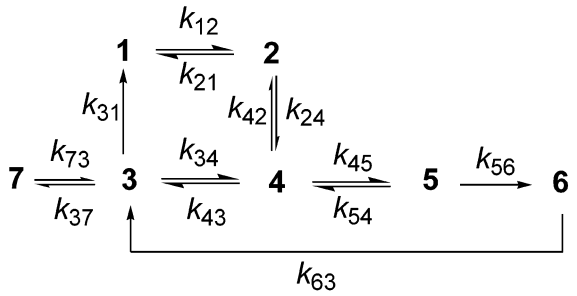

Taking the derivative of this expression gives

$$\left(\frac{\partial c_P(x,t)}{\partial t}\right)_{x=0} = \frac{1}{nFAD_P^{1/2}}\frac{d^{(1/2)}}{dt^{(1/2)}}i_{cat}(t) \quad (30)$$

so that the rate of product formation at the electrode surface is proportional to the semi-derivative of the current. Since $(\partial c_P(x,t)/\partial t)_{x=0}$ is proportional to the semi-derivative of the current or flux, eq 30 suggests that when the catalytic voltammogram has a sigmoidal or "steady-state" shape, $(\partial c_P(x,t)/\partial t)_{x=0}$ will exhibit tailing similar to a diffusional linear sweep voltammogram and when the catalytic voltammogram exhibits diffusional tailing, e.g., where mass transport of substrate becomes limiting, $(\partial c_P(x,t)/\partial t)_{x=0}$ will have a Gaussian peak shape.

As this discussion shows, even simple mechanisms such as the classical Michaelis−Menten mechanism lead to interpretive problems in electrochemical driven systems. Derivation of thermodynamic and kinetic data from experimental data requires four assumptions that do not necessarily hold in reality, i.e.,

(1) the surface coverage of ES is constant (steady state);

(2) surface concentration of substrate $c_s(0,t) = c_s^*$ (bulk concentration);

(3) the enzyme exists in only two forms, in the above example E and ES;

4) $i(t) \cong i_{cat}(t)$, i.e., the contributions to the current from other reactions are insignificant.

It is unclear to what extent the breakdown of these assumptions affects an accurate determination of K_m and k_2.

(ii) Finite Difference Method. For more complicated mechanisms, such as the general multistep mechanism shown in Scheme 1, a closed-form analytical solution is not obtainable. In this section, we demonstrate a finite difference numerical solution. To illustrate the finite difference method, we have simulated a hypothetical enzyme obeying Michaelis−Menten kinetics such as the system shown in eq 21 and we apply this method in the modeling of experimental data that we have acquired with a complex bacterial molybdoenzyme XDH.

At the potentials where catalysis occurs, we propose that our model enzyme can exist in seven possible states, which are shown in Scheme 2 along with the rate constants for the transitions between each state. Note that redox reactions involving electron relays within the enzyme are ignored, i.e., they are assumed to be non-rate-limiting.

The rate equations for the reaction scheme are

$$\frac{dx_1}{dt} = -k_{12}x_1 + k_{21}x_2 + k_{31}x_3$$

$$\frac{dx_2}{dt} = k_{12}x_1 - (k_{21} + k_{24})x_2 + k_{42}x_4$$

$$\frac{dx_3}{dt} = -(k_{31} + k_{34} + k_{37})x_3 + k_{43}x_4 + k_{53}x_5$$

$$\frac{dx_4}{dt} = k_{24}x_2 + k_{43}x_3 + (k_{42} + k_{43} + k_{45})x_4 + k_{54}x_5$$

$$\frac{dx_5}{dt} = k_{45}x_4 - (k_{54} + k_{53})x_5$$

$$\frac{dx_6}{dt} = k_{56}x_5 - k_{63}x_6$$

$$\frac{dx_7}{dt} = k_{37}x_3 - k_{73}x_7 \tag{31}$$

Multiplying throughout by $RT\Delta t/F\Delta E$, the finite difference forms of eq 31 are

$$\frac{RT}{F}\frac{\Delta x_1}{\Delta E} = -m_{12}x_1 + m_{21}x_2 + m_{31}x_3$$

$$\frac{RT}{F}\frac{\Delta x_2}{\Delta E} = m_{12}x_1 - (m_{21} + m_{24})x_2 + m_{42}x_4$$

$$\frac{RT}{F}\frac{\Delta x_3}{\Delta E} = -(m_{31} + m_{34} + m_{37})x_3 + m_{43}x_4 + m_{53}x_5$$

$$\frac{RT}{F}\frac{\Delta x_4}{\Delta E} = m_{24}x_2 + m_{43}x_3 + (m_{42} + m_{43} + m_{45})x_4 + m_{54}x_5$$

$$\frac{RT}{F}\frac{\Delta x_5}{\Delta E} = m_{45}x_4 - (m_{54} + m_{53})x_5$$

$$\frac{RT}{F}\frac{\Delta x_6}{\Delta E} = m_{56}x_5 - m_{63}x_6$$

$$\frac{RT}{F}\frac{\Delta x_7}{\Delta E} = m_{37}x_3 - m_{73}x_7 \tag{32}$$

with

$$m_i = \frac{RT}{Fv}k_i = \frac{k_i}{\sigma} = \frac{RT\Delta t}{F\Delta E}k_i \tag{33}$$

For the $(k + 1)$th time increment, $\Delta x = x^{k+1} - x^k$, the implicit finite difference form of eq 32 becomes

$$x_1{}^k = (1 + \tau m_{12})x_1^{k+1} - \tau m_{21}x_2^{k+1} - \tau m_{31}x_3^{k+1}$$

$$x_2{}^k = -\tau m_{12}x_1^{k+1} + (1 + \tau(m_{21} + m_{24}))x_2^{k+1} - \tau m_{42}x_4^{k+1}$$

$$x_3{}^k = (1 + \tau(m_{31} + m_{34} + m_{37}))x_3^{k+1} - \tau m_{43}x_4^{k+1} - \tau m_{53}x_5^{k+1}$$

$$x_4{}^k = -\tau m_{24}x_2^{k+1} - m_{34}x_3^{k+1} + (1 + \tau(m_{42} + m_{43} + m_{45}))x_4^{k+1} - \tau m_{54}x_5^{k+1}$$

$$x_5{}^k = -\tau m_{45}x_4^{k+1} + (1 + \tau(m_{54} + m_{53}))x_5^{k+1}$$

$$x_6{}^k = -\tau m_{56}x_5^{k+1} + (1 + \tau m_{63})x_6^{k+1}$$

$$x_7{}^k = -\tau m_{37}x_3^{k+1} + (1 + \tau m_{73})x_7^{k+1} \tag{34}$$

with

$$\tau = \frac{F\Delta E}{RT} \tag{35}$$

The substrate binding steps in Scheme 2 are second-order reactions, so k for those steps will be given by $k_i = k_i' c_S(0,t)$, with k_i' as a second-order rate constant and $c_S(0,t)$ as the concentration of substrate at the electrode surface, which for linear sweep voltammetry is given by eq 10. For the proposed mechanism, the flux of substrate at the electrode surface will be

$$-J_S(0,t) = D_S\left(\frac{\partial c_S(x,t)}{\partial x}\right)_{x=0} = k_{34}'c_S(0,t)\Gamma_E - k_{43}\Gamma_{ES} + k_{12}'c_S(0,t)\Gamma_{E'} - k_{21}\Gamma_{E'S} \tag{36}$$

The diffusion space is represented as a grid comprising m space increments and n time increments. Thus a concentration $c_S(x,t)$ is represented on the grid as $c_S(j,k)$ with j and k being distance and time indices, respectively, $1 \le j \le m$ and $1 \le k \le n$. The three-point finite difference form of the concentration gradient is

$$\left(\frac{\partial c_S(x,t)}{\partial x}\right)_{x=0} \cong -c_S^*\frac{3\mathbf{c}_1{}^k - 4\mathbf{c}_2{}^k + \mathbf{c}_3{}^k}{2\Delta x} \tag{37}$$

where $\mathbf{c}_j^k$ is the dimensionless concentration of the substrate obtained by dividing the concentration $c_S(j,k)$ by the bulk concentration of substrate, c_S^*, for example, $\mathbf{c}_1^{k+1} = c_S(0,t)/c_S^*$. The concentration profile of the substrate is simulated by solving eq 6. The implicit finite difference form of eq 6 is a set of linear equations[13]

$$-\mathbf{D}\mathbf{c}_1^{k+1} + (1 + 2\mathbf{D})\mathbf{c}_2^{k+1} - \mathbf{D}\mathbf{c}_3^{k+1} = \mathbf{c}_2{}^k$$

$$-\mathbf{D}\mathbf{c}_2^{k+1} + (1 + 2\mathbf{D})\mathbf{c}_3^{k+1} - \mathbf{D}\mathbf{c}_4^{k+1} = \mathbf{c}_3{}^k$$

$$-\mathbf{D}\mathbf{c}_3^{k+1} + (1 + 2\mathbf{D})\mathbf{c}_4^{k+1} - \mathbf{D}\mathbf{c}_5^{k+1} = \mathbf{c}_4{}^k$$

$$\vdots$$

$$-\mathbf{D}\mathbf{c}_{j-1}^{k+1} + (1 + 2\mathbf{D})\mathbf{c}_j^{k+1} - \mathbf{D}\mathbf{c}_{j+1}^{k+1} = \mathbf{c}_j{}^k$$

$$\vdots$$

$$-\mathbf{D}\mathbf{c}_{m-2}^{k+1} + (1 + 2\mathbf{D})\mathbf{c}_{m-1}^{k+1} = \mathbf{c}_{m-1}^k + \mathbf{D}\mathbf{c}_m^{k+1} \tag{38}$$

where $\mathbf{D}$ is a dimensionless parameter defined as

$$\mathbf{D} = \frac{D_S\Delta t}{(\Delta x)^2} \tag{39}$$

Substituting eq 37 into eq 36, multiplying through by $RT\Delta t/F\Delta E$ (i.e., $\Delta t/\tau$), and making the concentrations in eq 36 dimensionless gives

$$-\frac{D_S\Delta t c_S^*}{\tau}\frac{3\mathbf{c}_1^{k+1} - 4\mathbf{c}_2^{k+1} + \mathbf{c}_3^{k+1}}{2\Delta x} = m_{34}'c_S^*\mathbf{c}_1^{k+1}\Gamma_E - m_{43}\Gamma_{ES} \tag{40}$$

Combining and rearranging eqs 40 and 34 gives the system of equations to be solved for the catalytic reactions at the electrode surface

$$x_1^{\,k} = (1 + \tau m'_{12} c_S^* \mathbf{c}_1^{k+1}) x_1^{k+1} - \tau m_{21} x_2^{k+1} - \tau m_{31} x_3^{k+1}$$

$$x_2^{\,k} = -\tau m'_{12} c_S^* \mathbf{c}_1^{k+1} x_1^{k+1} + (1 + \tau(m_{21} + m_{24})) x_2^{k+1} - \tau m_{42} x_4^{k+1}$$

$$x_3^{\,k} = (1 + \tau(m_{31} + m'_{34} c_S^* \mathbf{c}_1^{k+1} + m_{37})) x_3^{k+1} - \tau m_{43} x_4^{k+1} - \tau m_{53} x_5^{k+1}$$

$$x_4^{\,k} = -\tau m_{24} x_2^{k+1} - \tau m'_{34} c_S^* \mathbf{c}_1^{k+1} x_3^{k+1} + (1 + \tau(m_{42} + m_{43} + m_{45})) x_4^{k+1} - \tau m_{54} x_5^{k+1}$$

$$x_5^{\,k} = -\tau m_{45} x_4^{k+1} + (1 + \tau(m_{54} + m_{53})) x_5^{k+1}$$

$$x_6^{\,k} = -\tau m_{56} x_5^{k+1} + (1 + \tau m_{63}) x_6^{k+1}$$

$$x_7^{\,k} = -\tau m_{37} x_3^{k+1} + (1 + \tau m_{73}) x_7^{k+1}$$

$$0 = -\tau m_{21} x_2^{k+1} - \tau m_{43} x_4^{k+1} + (\tau m'_{12} c_S^* x_1^{k+1} + \tau m'_{34} c_S^* x_3^{k+1} + 3\gamma) \mathbf{c}_1^{k+1} - 4\gamma \mathbf{c}_2^{k+1} + \gamma \mathbf{c}_3^{k+1} \quad (41)$$

with

$$\gamma = \frac{D_S \Delta t c_S^*}{2 \Delta x \Gamma_T} \quad (42)$$

Combining eqs 41 and 38 gives a system of nonlinear equations to be solved at each time increment to simulate the catalytic reaction

$$(1 + \tau m'_{12} c_S^* \mathbf{c}_1^{k+1}) x_1^{k+1} - \tau m_{21} x_2^{k+1} - \tau m_{31} x_3^{k+1} = x_1^{\,k}$$

$$-\tau m'_{12} c_S^* \mathbf{c}_1^{k+1} x_1^{k+1} + (1 + \tau(m_{21} + m_{24})) x_2^{k+1} - \tau m_{42} x_4^{k+1} = x_2^{\,k}$$

$$(1 + \tau(m_{31} + m'_{34} c_S^* \mathbf{c}_1^{k+1} + m_{37})) x_3^{k+1} - \tau m_{43} x_4^{k+1} - \tau m_{53} x_5^{k+1} = x_3^{\,k}$$

$$-\tau m_{24} x_2^{k+1} - \tau m'_{34} c_S^* \mathbf{c}_1^{k+1} x_3^{k+1} + (1 + \tau(m_{42} + m_{43} + m_{45})) x_4^{k+1} - \tau m_{54} x_5^{k+1} = x_4^{\,k}$$

$$-\tau m_{45} x_4^{k+1} + (1 + \tau(m_{54} + m_{53})) x_5^{k+1} = x_5^{\,k}$$

$$-\tau m_{56} x_5 + (1 + \tau m_{63}) x_6 = x_6^{\,k}$$

$$-\tau m_{37} x_3^{k+1} + (1 + \tau m_{73}) x_7^{k+1} = x_7^{\,k}$$

$$-\tau m_{21} x_2^{k+1} - \tau m_{43} x_4^{k+1} + (\tau m'_{12} c_S^* x_1^{k+1} + \tau m'_{34} c_S^* x_3^{k+1} + 3\gamma) \mathbf{c}_1^{k+1} - 4\gamma \mathbf{c}_2^{k+1} + \gamma \mathbf{c}_3^{k+1} = 0$$

$$-\mathbf{D}\mathbf{c}_1^{k+1} + (1 + 2\mathbf{D})\mathbf{c}_2^{k+1} - \mathbf{D}\mathbf{c}_3^{k+1} = \mathbf{c}_2^{\,k}$$

$$-\mathbf{D}\mathbf{c}_2^{k+1} + (1 + 2\mathbf{D})\mathbf{c}_3^{k+1} - \mathbf{D}\mathbf{c}_4^{k+1} = \mathbf{c}_3^{\,k}$$

$$-\mathbf{D}\mathbf{c}_3^{k+1} + (1 + 2\mathbf{D})\mathbf{c}_4^{k+1} - \mathbf{D}\mathbf{c}_5^{k+1} = \mathbf{c}_4^{\,k}$$

$$\vdots$$

$$-\mathbf{D}\mathbf{c}_{j-1}^{k+1} + (1 + 2\mathbf{D})\mathbf{c}_j^{k+1} - \mathbf{D}\mathbf{c}_{j+1}^{k+1} = \mathrm{c}_j^{\,k}$$

$$\vdots$$

$$-\mathbf{D}\mathbf{c}_{m-2}^{k+1} + (1 + 2\mathbf{D})\mathbf{c}_{m-1}^{k+1} = \mathbf{c}_{m-1}^{k} + \mathbf{D}\mathbf{c}_m^{k+1} \quad (43)$$

Since from eq 39

$$\Delta x = \left(\frac{D\Delta t}{\mathbf{D}}\right)^{1/2} = \left(\frac{D\tau}{\mathbf{D}\sigma}\right)^{1/2} \quad (44)$$

γ becomes

$$\gamma = \frac{c_S^*}{2\Gamma_T}\left(\frac{\mathbf{D}D\tau}{\sigma}\right)^{1/2} \quad (45)$$

The left-hand side of eq 43 can be written as the dot product of a sparse matrix, $\boldsymbol{A}$, and a column vector, $\boldsymbol{x}$, containing the concentrations of substrate and different redox forms of the enzyme $\boldsymbol{A}\cdot\boldsymbol{x} = \boldsymbol{b}$. Equation 43 can be solved using sparse matrix solving methods. The system of equations is nonlinear. The elements of the matrix containing electrochemical rate constants must be updated at each time increment. At each time step, one or more iterations can be made until the desired degree of precision is required.

Experimental Section

Details of enzyme preparation and cyclic voltammetry have been given previously.[19] The electroactive coverage, Γ_T, of the enzyme was determined by integrating the nonturnover peaks. The code to solve the fully implicit finite difference equations shown in eq 43 was written in Mathematica V5.0.[13,20] An expanding space grid was used in order to reduce the computation time as is customary for electrochemical problems.[11−13] Modifications to eq 43 required on an expanding space grid are detailed in Supporting Information. All simulations were performed using Mathematica V5.0[13,20] on an Apple Powerbook G4 computer with OS X 10.3 system software, a clock speed of 1 GHz and 512 MB of RAM. The system software (checked using the OX X 10.3 activity monitor utility) allocated a maximum of 36 MB of real memory and 230 MB virtual memory to Mathematica. The sparse matrix solver in Mathematica V5.0 uses UMFPACK multifrontal direct solver methods and when advantageous uses Krylov iterative methods preconditioned by an incomplete LU factorization.[21]

The nonlinear set of equations were iterated at each time step until the mean difference between elements on the finite difference grid between iterations was less than 10^{-10}. Some typical timings for computations carried out are shown below in Table 1.

Results

(i) Michaelis−Menten Kinetics. Simulations of a Michaelis−Menten mechanism shown in eq 21 were carried out under a wide range of substrate concentrations (Table 2).

The simulation results shown in Figure 2 confirm that the surface concentration of substrate differs from the bulk con-

TABLE 1: Indicative Computation Times

matrix size	time steps	computation time (s)
42 × 42	800	3.6
42 × 42	1600	6.5
57 × 57	1600	7.8
65 × 65	1600	8.3

TABLE 2: Michaelis−Menten Kinetics Simulation Parameters

variable	meaning	value
k_s (s^{-1})	heterogeneous rate constant	10
k_{+1} (M^{-1} s^{-1})	substrate binding rate constant	1.0×10^5
k_{-1} (s^{-1})	complex dissociation rate constant	1.0×10^{-2}
k_2 (s^{-1})	catalytic turnover number	25
Γ_T (mol cm^{-2})	surface coverage	1.0×10^{-11}
v (mV s^{-1})	voltammetric sweep rate	50
K_m (μM)	Michaelis constant	250

centration. As a guide, the greater the degree of tailing exhibited by the catalytic voltammogram the greater the difference. The bottom plot in Figure 2 shows that the rate of product formation is the semi-derivative of the current. The simulation provides the opportunity to extract apparent values of K_m and k_2 from plots of simulated current density vs substrate concentration using eq 46

$$j = \frac{nFk_2\Gamma_T c_S^*}{K_m + c_S^*} \tag{46}$$

These values can be compared to actual values of K_m and k_2 extracted using eq 25. Figure 3 shows the plots of simulated current density vs both the surface and bulk concentrations of substrate.

TABLE 3: Parameters Derived from Simulated Michaelis−Menten Kinetics

variable	value
$K_m{}^a$ (μM)	296 ± 4
$k_2{}^a$ (s^{-1})	25.0 ± 0.3
$K_m{}^b$ (μM)	490 ± 10
$k_2{}^b$ (s^{-1})	28.0 ± 0.6

[a] Recovered using eq 25 from a plot of simulated current density vs surface concentration of substrate $c_S(0,t)$, measured at the current maximum. [b] Recovered using eq 46 from a plot of simulated current density versus bulk concentration of substrate, c_S^*.

Although the values of k_2 recovered from the plots shown in Figure 3 are similar, the value of K_m recovered using eq 46 is twice the value used in the simulation, an observation attributable to the failure of the steady-state assumption.

Figure 4 shows the variation of fractional surface coverage of the different forms of the enzyme during the course of the experiment, again highlighting the breakdown of the steady-state assumption, i.e., the surface concentration of the intermediate species ES varies during the experiment.

Figure 5 shows the derivative of the plots shown in Figure 4. These plots have been normalized to the dimensionless current scale. The absence of a steady state for the enzyme−substrate complex is again noticeable.

(ii) Catalytic Electrochemistry of XDH. *Rhodobacter capsulatus* XDH is a multiredox center molybdoenzyme, whose direct catalytic electrochemistry we reported recently.[19] Similar to other members of the xanthine oxidase family, XDH catalyses the (2-electron) hydroxylation of some purines, e.g., xanthine to uric acid. This enzyme is interesting as it resembles XDH found in humans, and an important role for

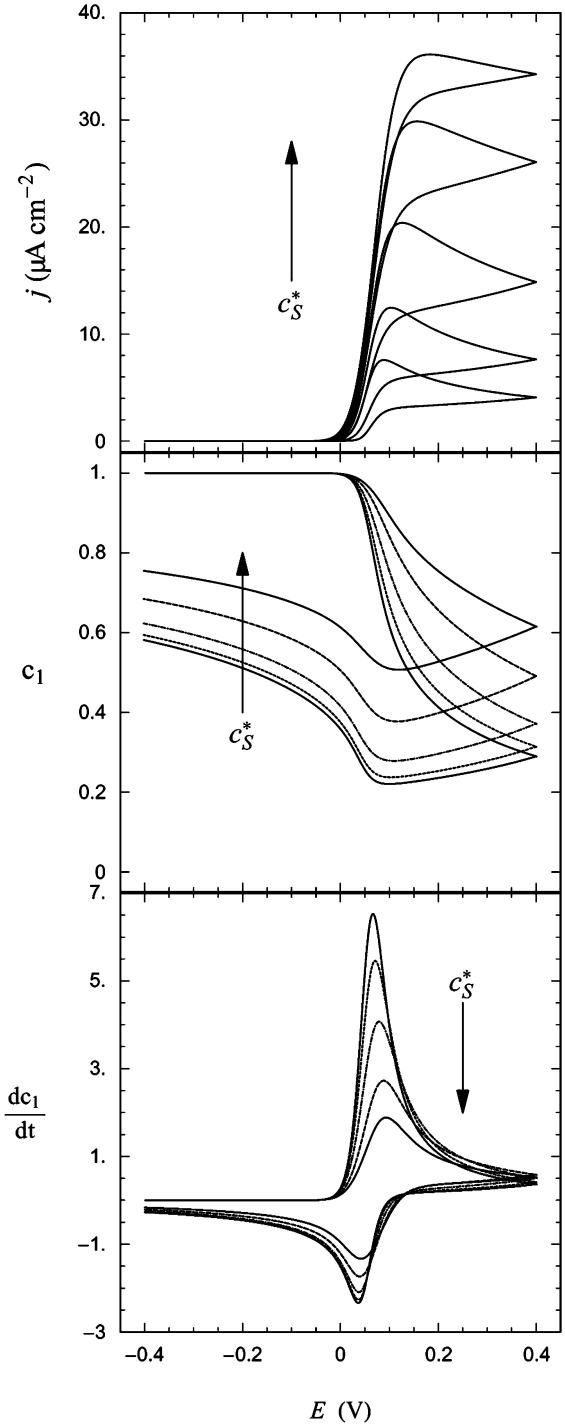

Figure 2. Plots of simulated catalytic voltammograms (top), $\mathbf{c}_1$, ($c_S(0,t)/c_S^*$), (center), and $d\mathbf{c}_1/dt$ (bottom), obtained from simulation with the parameters given in Table 2. Concentrations used in simulations were $c_S^* = 80$, 150, 300, 600, and 1000 μM. The top and center plots show output with c_S^* increasing in magnitude from bottom to top. The bottom plot shows output with c_S^* increasing in magnitude from top to bottom.

XDH and the related xanthine oxidase (XO) in medical conditions such as gout and hyperuricaemia has been proposed, and the conversion of XDH to XO is of major medical interest as it has been implicated in diseases characterized by oxygen-radical-induced tissue damage, such as postischaemic reperfusion injury.[22]

The electrochemistry of this bacterial XDH was found to be quite unusual both in the high potential at which catalysis was observed and also the catalytic waveform, which was distinctly

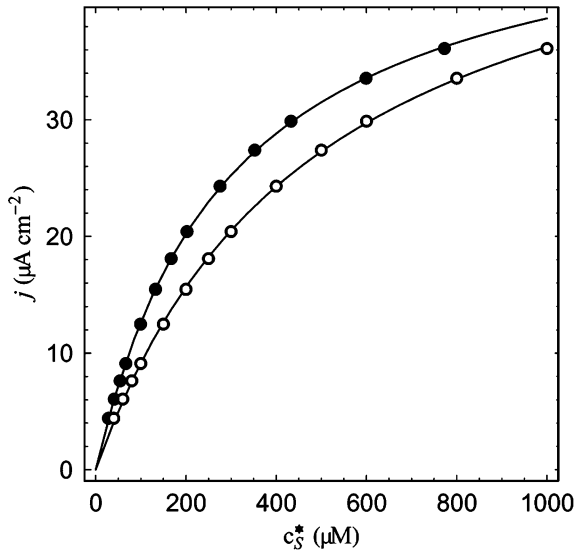

Figure 3. Plot of simulated current density versus $c_S(0,t)$ (top) and c_S^* (bottom). Points are simulated data points and lines represent a nonlinear fit of the data.

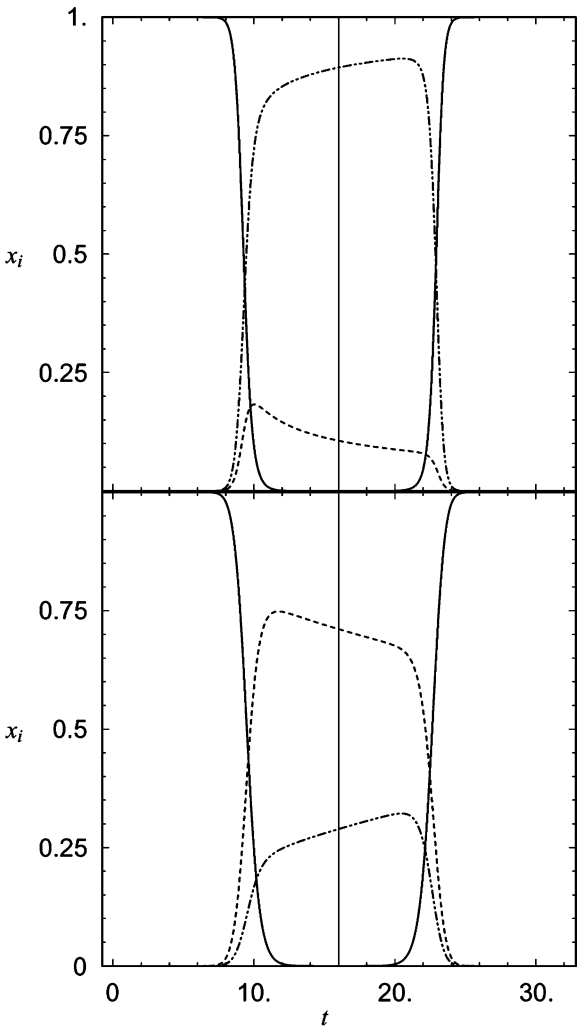

Figure 4. Plots of simulated x_i vs time. $x_{E'}$ (solid line), x_E (dot-dashed line), x_{ES} (dashed line) with $c_S^* = 80$ μM (top) and 1 mM (bottom).

peak shaped at room temperature. In this regard, it demanded a thorough analysis using the methods described here to enable a better understanding of the complex mechanism that is evidently occurring.

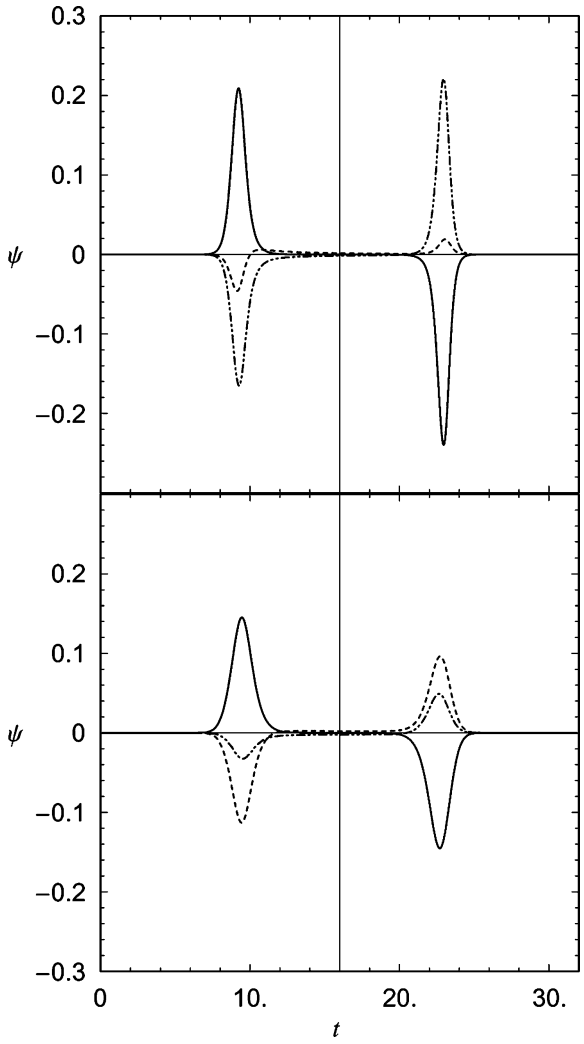

Figure 5. Plots of simulated ψ, $-\frac{RT}{F}\frac{dx_i}{dE}$, vs time. $x_{E'}$ (solid line), x_E (dot-dashed line), x_{ES} (dashed line) with $c_S^* = 80$ μM (top) and 1 mM (bottom).

The catalytic mechanism set out in Scheme 2 has been adapted to XDH and is shown in Scheme 3 with electrochemical steps shown as vertical transitions and chemical steps as horizontal transitions. The subscripted Roman numerals refer to the oxidation state of the molybdenum center. Here we have ignored the transient existence of the Mo^V form, which is a catalytically inactive intermediate. Although it is readily observed[23,24] in single turnover experiments as an intermediate during electron egress from the fully reduced Mo^{IV} form, (2-electron) substrate oxidation by necessity only involves the Mo^{VI} and Mo^{IV} states, and the catalytic role of the half reduced form is still open to debate.[25]

Although XDHs (and XOs) from a number of organisms have been extensively studied,[26,27] some differences between the homogeneous catalytic cycle and the electrochemically driven cycle are to be expected. As mentioned,[19] the electrochemically driven catalytic reaction occurs at a potential where all redox centers, including the Mo active site, will be fully oxidized. It was proposed that an (inactive) state of surface confined XDH is formed (E'_{VI} in Scheme 3) bearing a ring-opened tetrahydropterin and that the electrochemically driven catalytic cycle depends on an oxidative ring closure (k_{24}) to give the Michaelis complex E_{VI}·S. No electrochemical response was seen corresponding to this 2-electron ligand-based oxidation in the absence of substrate, hence k_{13} is ignored in Scheme 3. That is, we

SCHEME 3

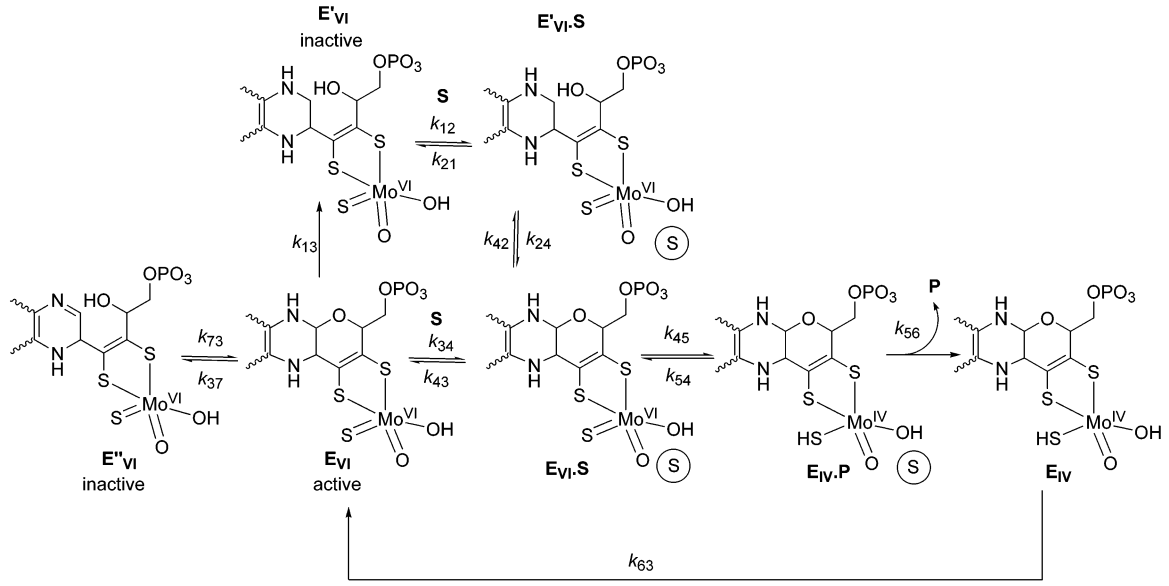

proposed that substrate (xanthine, S) binding (k_{12}) is a necessary trigger for this conformational change, which, in turn, enables the oxidative ring closure (k_{24}). After turnover (k_{45}), the product is released (k_{56}) and the enzyme is reoxidized rapidly to its resting state (k_{63}) via the Fe−S and FAD cofactors. The electrochemically driven catalytic reaction occurs ca. 1 V above the $Mo^{VI/IV}$ couple therefore extremely rapid reoxidation of the active site, via the cofactors, back to state 3 is expected,[28] i.e., $k_{63} \gg k_{56}$. Therefore, steps 5 → 6 and 6 → 3 were modeled as a single step 5 → 3 with rate constant k_{53}.

An additional deactivation step (k_{37}) is proposed to explain the conspicuous tailing of the catalytic waveform at high potential (Figure 6), which we propose corresponds again to a ring-opened form; in this case, the (oxidized) dihydropterin (E''_{VI}). This tailing is seen at room temperature, [19] but at 4 °C, a steady-state-like (sigmoidal) waveform is observed.[19]

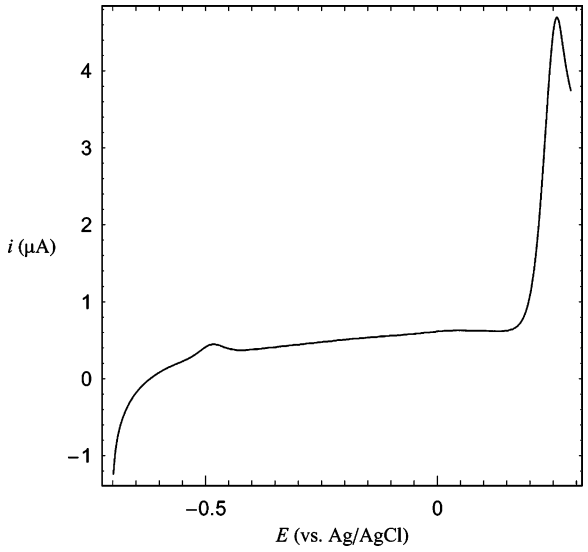

Figure 6. Voltammogram of XDH on an EPG electrode in a solution of 470 μM xanthine. The sweep rate was 5 mV s^{-1}. The peak at −0.5 V corresponds to the FAD cofactor.

Peak-shaped voltammetric responses normally indicate the electrochemical reaction of a surface bound species.[16,17] Increasing the rate of mass transport of substrate to the electrode by, e.g., agitating the cell, increases the current. This confirms that the observed peak shape is not solely due to the electrochemical reaction of a surface-bound species but contains a component that is governed by mass transport to the electrode, i.e., substrate turnover

TABLE 4: Simulation Parameters for the XDH System

variable	value
T (K)	298
v (mV s^{-1})	5
K_d (μM)	280
k_{21} (s^{-1})	140
k_{12} (M^{-1} s^{-1})	5.0×10^5
k_{45} (s^{-1})	180
k_{54} (s^{-1})	35
k_s (s^{-1})	>10
$E^{\circ\prime}$ (mV vs NHE)	445
Γ_T (mol cm^{-2})	5×10^{-12}
k_{37} (M^{-1} s^{-1})	1.0
k_{73} (s^{-1})	0.2
k_{53} (s^{-1})	250

To simulate the electrochemically driven XDH catalysis, we were guided by data published for chicken liver XDH.[26] Although obtained at 4 °C, we envisage these values to be useful guides. Initial simulations indicated that K_d for E′·S should be of a similar order of magnitude to that of E·S. Large differences in the K_d values produced catalytic peak shapes inconsistent with those experimentally obtained. Therefore, K_d was restrained to be the same for both forms of the enzyme. The electrochemical rates were all assumed to have the same electrochemical standard rate constant with the potential dependence of the rates described by Butler−Volmer kinetics. We found that standard rate constants greater than approximately 10 s^{-1} had little effect on the simulation results. Therefore, the adjustable parameters in the simulation were the redox potential ($E^{\circ\prime}$) at which oxidative ring closure (E′·S → E·S) occurred (governing the potential for onset of catalysis), the surface coverage of the enzyme, (determining the catalytic current), k_{53}, the rate constant for the overall conversion of E_{IV}·P to E_{VI}, and k_{37}, the rate constant for deactivation of the fully oxidized enzyme. The simulation parameters used are shown in Table 4.

After subtracting an extrapolated background, a simulation provided a good fit with the experimentally obtained voltam-

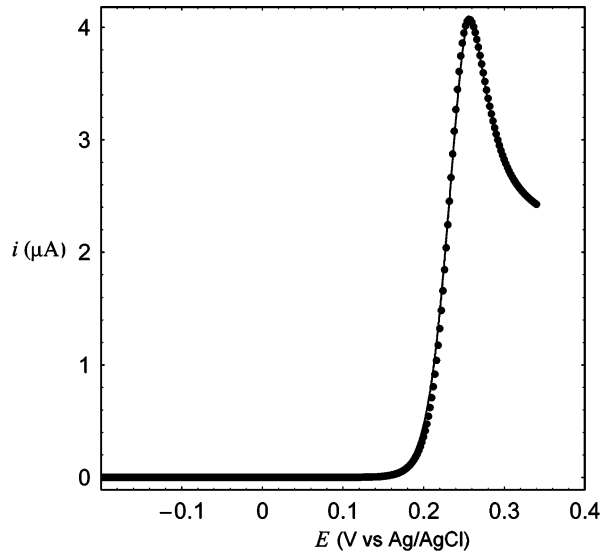

Figure 7. A portion of the voltammogram shown in Figure 6 with background subtracted (line) and a simulated catalytic voltammogram (dots).

mogram (Figure 7). Uncertainties remain about the proposed mechanism, such as the exact nature of the deactivation, but the ring-opening hypothesis is based on a significant associated conformational change at the active site whereby turnover ceases completely. The reason for this remains speculative, but it may be related to disruption of the intricate electron-transfer relay system (Mo → Fe−S → Fe−S → FAD) within the enzyme, thus disabling electron egress from the reduced Mo active site. Therefore, the simulation parameters in Table 4 should be regarded cautiously. Further research is being carried out to better understand the interesting mechanism of this complex metalloenzyme.

Acknowledgment. We would like to dedicate this paper to Steve Waugh on the occasion of his retirement. We gratefully acknowledge support of the Australian Research Council (DP0343405).

Supporting Information Available: Modifications to eq 43 required on an expanding space grid. This material is available free of charge via the Internet at http://pubs.acs.org.

References and Notes

(1) Armstrong, F. A.; Wilson, G. S. *Electrochim. Acta* **2000**, *45*, 2623−2645.
(2) Cass, A. E. G.; Davis, G.; Francis, G. D.; Hill, H. A. O.; Aston, W. J.; Higgins, I. J.; Plotkin, E. V.; Scott, L. D. L.; Turner, A. P. F. *Anal. Chem.* **1984**, *56*, 667−671.
(3) Wang, J. *Electroanalysis* **2001**, *13*, 983−988.
(4) Bartlett, P. N.; Tebbutt, P.; Whitaker, R. G. *Prog. React. Kinet.* **1991**, *16*, 55−155.
(5) Bartlett, P. N.; Pratt, K. F. E. *Biosens. Bioelect.* **1993**, *8*, 451−462.
(6) Limoges, B.; Moiroux, J.; Saveant, J. M. *J. Electroanal. Chem.* **2002**, *521*, 1−7.
(7) Limoges, B.; Moiroux, J.; Saveant, J. M. *J. Electroanal. Chem.* **2002**, *521*, 8−15.
(8) Limoges, B.; Saveant, J. M. *J. Electroanal. Chem.* **2003**, *549*, 61−70.
(9) Limoges, B.; Saveant, J. M. *J. Electroanal. Chem.* **2004**, *562*, 43−52.
(10) Britz, D. *Digital Simulation in Electrochemistry*; Springer-Verlag: Berlin, 1988.
(11) Rudolph, M. In *Physical Electrochemistry Principles, Methods, and Applications*; Rubenstein, I., Ed.; Marcel Dekker: New York, 1995; pp 81−130.
(12) Speiser, B. In *Electroanal. Chem.*; Bard, A. J., Rubenstein, I., Eds.; Marcel Dekker: New York, 1996; Vol. 19, pp 1−109.
(13) Honeychurch, M. J. *Simulating Electrochemical Reactions with Mathematica*; IBNH: Brisbane, 2004.
(14) Armstrong, F. A.; Bond, A. M.; Hill, H. A. O.; Psalti, I. S. M.; Zoski, C. G. *J. Phys. Chem.* **1989**, *93*, 6485−6493.
(15) Bard, A. J.; Faulkner, L. R. *Electrochemical Methods*, 2nd ed.; J. Wiley & Sons: New York, 2001.
(16) Honeychurch, M. J.; Rechnitz, G. A. *Electroanalysis* **1998**, *10*, 285−293.
(17) Honeychurch, M. J.; Rechnitz, G. A. *Electroanalysis* **1998**, *10*, 453−457.
(18) Baumann, G. *Mathematica in Education and Research* **1999**, *8*, 58−65.
(19) Aguey-Zinsou, K. F.; Bernhardt, P. V.; Leimkühler, S. *J. Am. Chem. Soc.* **2003**, *125*, 15352−15358.
(20) Wolfram, S. *The Mathematica Book*, 4th ed.; Cambridge University Press/Wolfram Media: New York/Champaign, 1999.
(21) Press: W. H.; Teukolsky, S. A.; Vetterling, W. T.; Flannery, B. P. *Numerical Recipes in C*, 2nd ed.; Cambridge University Press: Cambridge, 1992.
(22) Harrison, R. *Free Radical Biol. Med.* **2002**, *33*, 774−797.
(23) Hille, R.; Kim, J. H.; Hemann, C. *Biochemistry* **1993**, *32*, 3973−3980.
(24) Kim, J. H.; Ryan, M. G.; Knaut, H.; Hille, R. *J. Biol. Chem.* **1996**, *271*, 6771−6780.
(25) Stockert, A. L.; Shinde, S. S.; Anderson, R. F.; Hille, R. *J. Am. Chem. Soc.* **2002**, *124*, 14554−14555.
(26) Hille, R. *Chem. Rev.* **1996**, *96*, 2757−2816.
(27) Hille, R. *J. Biol. Inorg. Chem.* **1996**, *1*, 397−404.
(28) Honeychurch, M. J. *Langmuir* **1999**, *15*, 5158−5163.